The Three-Dimensional Distribution of Galactic AGB Stars with ALLWISE

Nicholas M. Hunt-Walker, Željko Ivezić, Andrew C. Becker

University of Washington, Department of Astronomy, Seattle, WA 98195

nmhw@uw.edu, ivezic@uw.edu, acbecker@uw.edu

1. Introduction

The structure of the Milky Way holds clues to the processes of formation and evolution of galaxies. Historical models typically assumed three discrete components described by simple analytic expressions: the thin disk, thick disk, and halo (Bahcall & Soneira 1980; Gilmore et al. 1989; Majewski 1993). Recent surveys, such as the Sloan Digital Sky Survey (SDSS, York et al. 2000) and the Two Micron All Sky Survey (2MASS, Skrutskie et al. 2006), have provided much more detail about these components. For example, SDSS data have constrained stellar distributions in the 7-dimensional space spanned by spatial coordinates (Jurić et al. 2008), velocity components (Bond et al. 2010), and metallicity (Ivezić et al. 2008). The resulting maps revealed rich, complex substructure in the distribution of the Milky Way's stars (e.g. Ivezić et al. 2000; Yanny et al. 2000; Vivas et al. 2001; Newberg et al. 2002; Majewski et al. 2003; Belokurov et al. 2006; Grillmair 2006; Vivas & Zinn 2006), deeply shaking the older view of a smooth Galaxy.

The large distance limit of about 100 kpc for some halo populations (e.g. RR Lyrae and BHB stars with SDSS, Sesar et al. 2010 and red giants with 2MASS, Majewski et al. 2003), as well as about 10 kpc for very numerous main sequence stars, is not reached when studying disk component at low galactic latitudes. As shown, for example, by Berry et al. (2012), the extinction due to interstellar dust limits the SDSS sample of main sequence stars to heliocentric distances of only a few kpc. In order to avoid detrimental effect of dust extinction, stellar samples need to be probed at longer infrared wavelengths. Several infrared surveys covering the Galactic plane have recently become available (WISE, Wright et al. 2010; Cutri et al. 2012, GLIMPSE Churchwell et al. 2009; Benjamin et al. 2003, VVV Saito et al. 2012).

Among populations suitable for studying Galactic structure using infrared surveys, Asymptotic Giant Branch (AGB) stars stand out. AGB stars represent the last stage of evolution for stars between 0.8 and 8 $M_{\odot}$ (Iben & Renzini 1983; Herwig 2005). Stars from this mass range can reach the final stages of stellar evolution within the Galactic timescale (∼10 Gyr, Iben & Renzini 1983) and thus are bound to reside throughout the Galaxy wherever other stars are present. This phase of stellar evolution is marked by two distinct episodes with different observational characteristics: the early AGB phase (E-AGB) and the thermally-pulsing AGB phase (TP). During the thermally-pulsing phase, AGB stars produce substantial dust-driven stellar winds ($10^{-7} < \dot{M} < 10^{-4}$ $M_{\odot}$ yr^{-1}, Olofsson et al. 2002) rich in oxides (SiO, Al_2O_3, etc.) or carbon-rich molecules (SiC, amC, etc.). The dominant chemical composition is highly dependent upon the metallicity of the host

galaxy (Matsuura et al. 2005). High-metallicity galaxies like the Milky Way have a substantial population of oxygen-rich AGB stars (Habing et al. 1985), whereas low-metallicity galaxies such as the Magellanic clouds are dominated by carbon-rich AGB stars (Boyer et al. 2011). In both cases, the other species of AGB star is rarely seen, as richness in one chemical type (e.g. oxides) necessitates the almost complete capture of the other chemical type (e.g. carbon) in CO (Iben & Renzini 1983).

The dust-rich winds in TP phase create vast circumstellar shells that are warmed by the stellar photosphere and emit copiously in the near- and mid-infrared (NIR & MIR, respectively). Together with high bolometric luminosity (10^3–10^4 $M_\odot$, Knauer et al. 2001), this redistribution of the output radiation to the infrared wavelength makes AGB stars excellent disk probe when infrared survey data are available. Indeed, they were detected all the way to the Galactic center even with the IRAS survey (Jackson et al. 2002). Such disk studies can now be significantly improved thanks to the much more sensitive WISE survey.

The *Wide-field Infrared Survey Explorer*, WISE, is a space observatory that has imaged essentially the entire sky in the MIR (3.4, 4.6, 12, and 22 μm). The WISE catalog has been positionally matched to the 2MASS catalog, with the matched catalog listing NIR and MIR 7-band photometry for hundreds of millions of sources. Given the depths of the two surveys, this catalog should contain AGB stars to many kpc beyond the Galactic center. Here we develop selection methods for AGB stars using WISE and 2MASS data, and analyse the resulting samples.

In Section 2, we describe in detail the WISE, 2MASS and other auxiliary data used in our study and the data reduction process. In Section 3, we use samples of known Galactic and Magellanic AGB stars to derive WISE-2MASS color-based selection criteria, and calibrate color-absolute magnitude relations. In Section 4, we describe the spatial density distribution of selected AGB candidates from the Milky Way. Our conclusions are summarized in Section 5.

2. Input Catalogs and Data Preparation

Our principal data source is the merged WISE-2MASS catalog. In order to derive WISE-2MASS color-based selection criteria, we use a homogenous sample of AGB stars from the OGLE-III Catalog of Variable Stars supplying objects in the Magellanic Clouds. This sample serves to calibrate color-color and color-absolute magnitude relations that underlie our distance estimates. In order to assess what infrared populations could contribute to contamination of selected AGB candidates, we utilize stellar and extragalactic sources from SDSS data release 7 pulled from the NYU Value-added Galaxy Catalog, the SDSS unofficial Luminous Red Galaxy sample, young stellar objects identified in WISE data, and red giant branch stars from the OGLE-III Catalog of Variable Stars, also described below. We conclude this section by describing how these auxiliary catalogs were positionally merged with the WISE-2MASS catalog, summarize the object counts before and after quality control (Table 1), and summarize the effects of WISE-2MASS color-color cuts (Table 2)

on the AGB and contaminant samples.

2.1. WISE-2MASS catalog

In this study, we rely heavily on data from the ALLWISE extension of the WISE survey, combining data from the initial All-Sky Data Release, the 3-band cryogenic data release, and the NEOWISE post-cryogenic data release (Cutri et al. 2013). The initial WISE All-Sky Data Release observed the sky between January and August 2010, observing the sky 1.2 times on average with four detectors, operating at 3.4, 4.6, 12, and 22μm. Hereon we refer to ALLWISE photometric bands at [3.4μm/4.6μm/12μm/22μm] as [$W1/W2/W3/W4$]. The positions of objects in the WISE catalog were calibrated using the 2MASS point source catalog.

The 3-band cryogenic data release contains data from $W1$, 2, and 3, and surveyed 30% of the sky between August and October 2010. During the 3-band cryogenic survey, $W1$ and $W2$ operated with nearly the same sensitivity as during the full survey. Warming of the telescope reduced sensitivity in $W3$ and fully saturated $W4$. The NEOWISE post-cryogenic data release contains $W1$ and $W2$ measurements, with sensitivities close to those obtained during the full cryogenic phase. During this phase, WISE surveyed 70% of the sky. Data products from the post-cryogenic release included updated instrumental, astrometric, and photometric calibrations and reduction algorithms, resulting in higher signal-to-noise for most sources. The overall number of sources compiled into ALLWISE totals over 747.6 million.

2.2. Variable Giants from the OGLE-III Catalog of Variable Stars

The OGLE-III Catalog of Variable Stars (CVS) (Udalski et al. 2008; Soszyński et al. 2009, 2011) is a subset of the overall OGLE-III dataset, containing roughly 10 years of observations in the V- and I-bands of over 120,000 variable stars, with typically 700-900 data points per star in the I-band and about 50 data points per star in V-band. With high-precision photometry (~ 0.01 mag, Soszynski et al. 2007), these observations saturate at $I = 12.5$ mag, and are limited at the faint end at $I = 20.5$ mag (Zebrun et al. 2001). The variability of these stars covers a wide range of periodicity ($4 < P < 2000$ days) and amplitudes ($0.005 < A_I < 5.7$ mag).

The OGLE-III CVS is accessible through an online database[1], with long-period variables (LPVs) classified by object type, evolutionary status , and spectral type.

[1] http://ogledb.astrouw.edu.pl/~ogle/CVS/

2.2.1. AGB Stars

Stars brighter than the tip of the red giant branch (RGB) ($K_s < 12.05$ mag in LMC; Soszynski et al. 2004, 2007) are classified as AGBs. Object types (OSARG, Mira, SRV) are based chiefly on variability and luminosity. OGLE Small Amplitude Red Giants (hereon OSARGs) are weakly-variable ($0.005 < A_I < 0.13$ mag), with relatively short periods ($10 < P < 100$ days; Soszynski et al. 2004). Additionally, because these objects are multiperiodic, OSARGs are selected using their period ratios and their distances from established period-luminosity ($\log P - L$) sequences from Wood et al. (1999). For a more detailed description of their selection, see Soszynski et al. (2007). Mira variables and Semi-Regular Variables (hereon SRVs) are identified using I-band amplitudes and $P - W_I$, where W_I is the reddening-free Wesenheit index (Soszynski et al. 2005):

$$W_I = I - 1.55(V - I) \quad (1)$$

For individual $\log(P) - L$ sequences, spectral type (O-rich or C-rich) is easily seen as separations in $\log(P) - L$ space as well as visible-NIR color-color space. The initial classifications are based on spectroscopically-observed stars and were extended more generally to $\log(P) - L$ and visible-NIR color-color criteria (Soszynski et al. 2005, 2007). This clear separation can be seen in Figure 1.

From the initial OGLE-III LMC sample of 46,467 LPVs we retain 44,013 after matching to ALLWISE within 3", and 43,247 after ensuring only 1 match to 2MASS. The I-band median of OGLE-III LPVs is ≈ 14.68 mag with a standard deviation of 0.72 mag, appearing well above the OGLE I-band 5σ faint limit. Out of the entire sample only 13 objects (Miras) fall below the 5σ faint limit, and 41 above the saturation limit. Because so few stars even approach the faint limit of OGLE, we expect the OGLE-2MASS catalog of AGBs to effectively represent the complete sample of AGB stars in the LMC down to $I < 20.5$, oscillating with amplitudes > 0.005 mag.

Out of the 43,247 objects matched to ALLWISE and 2MASS within 3", 1,633 are Mira variables, 30,756 are OSARGs, and 10,858 are SRVs. The distributions of these objects in $\log(P) - L$ and visible-NIR color-color space are summarized in Figure 2.

2.2.2. Red Giant Branch Stars

As RGBs can contaminate the same $\log(P) - L$ space and color-color space as AGB stars, we seek to use RGBs identified by the OGLE-III CVS to quantify their contamination of our AGB sample. Stars brighter than the tip of the RGB ($K_s < 12.05$ mag in LMC; Soszynski et al. 2004, 2007) are classified as AGBs. Below that threshold, narrow sequences of variable stars appear to share similar slopes and intercept with AGB stars above the TRGB. Soszynski et al. (2004) classifies these objects as RGBs. The OGLE-III CVS LMC sample initially contains 45,528 RGB stars. When matched to ALLWISE-2MASS catalog within 3" we retain 40,764 RGBs.

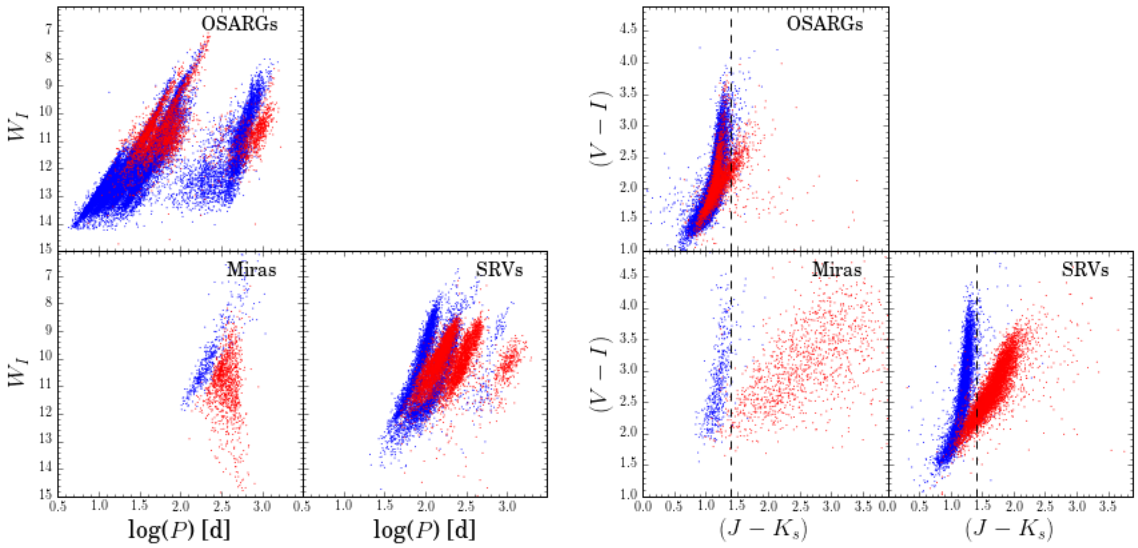

Fig. 1.— O-rich (*blue*) and C-rich (*red*) OGLE-III LPVs matched to 2MASS. *Left*: W_I vs log period in days. *Right:* OGLE-III $(V-I)$ vs 2MASS $(J-K_s)$. The dashed line represents $(J-K_s) = 1.4$.

2.3. Extragalactic catalogs from SDSS

SDSS is a multi-year survey of roughly 25% of the sky that collected both photometric (*u, g, r, i, z*-bands for 700+ million objects) and spectroscopic measurements (1.6+ million) of stars and extragalactic sources (York et al. 2000). Though its ground-based nature and sensitivity to interstellar extinction prevent SDSS from being an all-sky survey, it represents the largest spectrophotometric catalog to date. For this study we collect extragalactic objects from the NYU Value-added Galaxy Catalog, containing objects matched between SDSS and several auxiliary surveys spanning multiple wavelength regimes, and the SDSS Luminous Red Galaxy sample, isolating high-confidence luminous red galaxies from the SDSS database. The color-color distributions of these sample sets are shown in Figure 3.

2.3.1. The NYU Value-added Galaxy Catalog

In order to cull the full set of SDSS spectrophotometry and produce an easily-referenced extragalactic catalog for investigating galaxy formation and evolution, the NYU Value-added Galaxy Catalog (NYU-VAGC; Blanton et al. 2005) was created as of SDSS data-release 7 (DR7).

The NYU-VAGC contains matches between SDSS spectrophotometry and the following catalogs: the FIRST radio survey, the 2MASS Point Source Catalog, the 2MASS Extended Source Catalog, the Two-degree Field Galaxy Redshift Survey, the IRAS Point Source Catalog Redshift

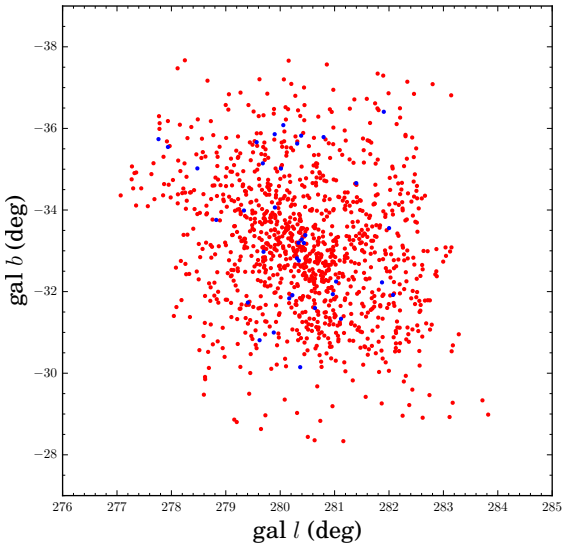

Fig. 2.— O-rich (*blue*) and C-rich (*red*) OGLE-III Miras with $(J - K_s) > 1.4$.

Survey, and Reference Catalog 3 (RC3.9b). As a consequence, the NYU-VAGC retains SDSS optical photometry in addition to spectral classifications (QSO, galaxy, star) and subclassifications (AGN, starforming galaxy, starburst galaxy, etc.) for 441,707 objects across 10,417 square degrees of the SDSS footprint. Main and secondary classifications are made by comparing measured optical spectra to the SDSS spectral library. See Blanton et al. (2005) for the full set of reduction and inclusion criteria. This catalog is available via an online data repository[2], along with a full description of the data and other subsamples not used in this study. The populations for each species (QSO, AGN, starforming galaxy (SF), starburst galaxy (SB)) are found in Table 1.

2.3.2. The Luminous Red Galaxy Sample

Subselected for the study of Baryon Acoustic Oscillations by Kazin et al. (2010), the Luminous Red Galaxy sample (LRGs; Eisenstein et al. 2001) is also sourced from SDSS DR7. LRGs contaminate the IR color-color space of AGB stars due to their large redshifts ($z \sim 0.3$). We obtain the LRG sample from the data repository[3] of Kazin et al. (2010). The initial sample is volume-limited, containing 105,631 objects spanning a redshift range of $0.16 < z < 0.47$.

[2] http://sdss.physics.nyu.edu/vagc/

[3] http://cosmo.nyu.edu/~eak306/SDSS-LRG.html

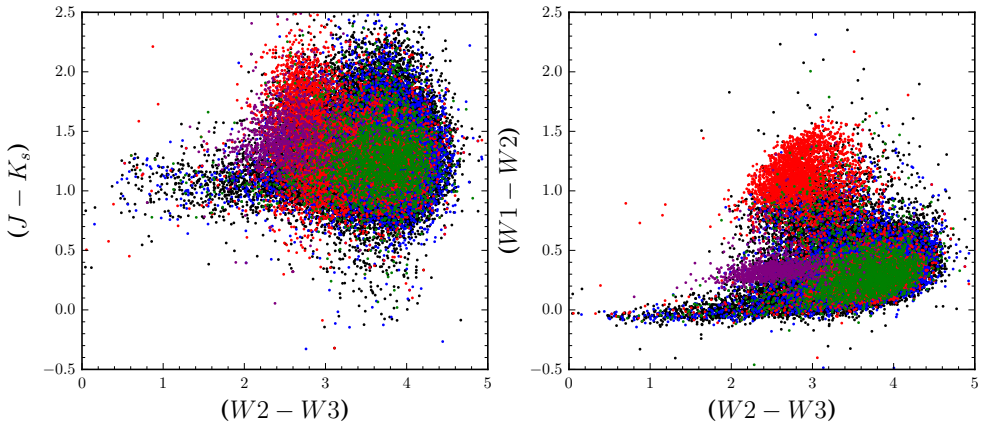

Fig. 3.— Extragalactic sources from SDSS DR7's VAGC and LRG samples. Objects are (*black*) starforming galaxies, (*blue*) starburst galaxies, (*red*) QSOs, (*green*) AGN, and (*purple*) LRGs.

2.4. WISE+2MASS Young Stellar Objects

Young Stellar Objects (YSOs) represent a unique contaminant in our search for dust-enshrouded AGB stars. Similar to AGBs, YSOs are luminous sources surrounded by warm, dusty environments. That warm dust can then glow brightly in the MIR, easily contaminating AGB color-color space. To characterize and later eliminate this potential contaminant, we select as our base sample 290 YSOs from Rebull et al. (2011), a survey searching for YSOs in the Taurus Molecular Cloud using data from WISE, ancillary data from SDSS and 2MASS, and covering 260 deg^2. As YSO tend to be embedded within high-extinction clouds, we expect that the dust-reddened NIR/MIR emission from these objects should match to similar objects in the LMC when we later calibrate our color-color criteria.

2.5. WISE+2MASS Stellar Locus

The color-color space occupied by AGB stars showing significant photospheric emission in WISE filters is heavily populated by naked stars from the main sequence (Nikutta et al. 2014). By sheer number, these stars would drown out sources that could be AGB stars with thin circumstellar envelopes. To address this, we extract the stellar locus from ALLWISE in the direction of the LMC ($276.5° < l < 284°$, $-38.2° < b < -28°$). We require that every object have one 2MASS association, $[W1/W2/W3]$ signal-to-noise > 1, detections in 2MASS J, H, and K_s, and confusion & contamination flags set to 0 for $[W1/W2/W3]$. We then adapt the color-color criteria from Davenport et al. (2014). Their locus focuses on stars with effective temperatures $3540 < T_{\rm eff} < 7200K$. We fit their criteria for $J-K_s$ vs $W1-W2$ within 3σ of the locus with degree-3 polynomials. The resulting fit for the 3σ stellar locus follows:

$$(J-K_s) < 61.67(W1-W2)^3 - 17.88(W1-W2)^2 + 1.68(W1-W2) + 0.99 \quad (2)$$
$$(J-K_s) > 40.19(W1-W2)^3 - 9.78(W1-W2)^2 + 0.54(W1-W2) + 0.64 \quad (3)$$

The resulting locus sample, as well as the original Davenport et al. (2014) bounds and locus are shown in in Fig 4. Note that our sample goes beyond the limits of the stated locus.

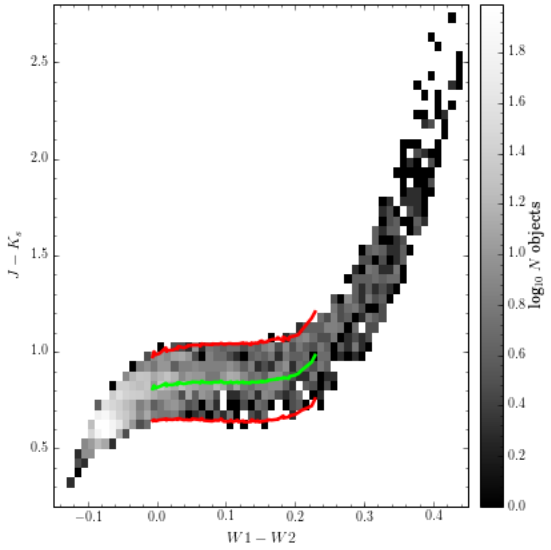

Fig. 4.— The WISE-2MASS stellar locus. (*black dots*) objects from the stellar locus in the direction of the LMC. (*green line*) WISE-2MASS color-color stellar locus derived from Davenport et al. (2014). (*red line*) 3σ boundaries for WISE-2MASS color-color locus.

2.6. Merged Samples

The OGLE-III AGB sample, as well as the SDSS and YSO samples, were matched to the ALLWISE data products via the `GATOR` tool at the NASA/IPAC Infrared Science Archive[4]. The accepted matching radius was 3" execept in the case of YSOs, which were limited to 1". YSO objects were obtained from the VIZIER service already possessing WISE observations, so we were able to accept a smaller matching radius as we only sought the extra 2MASS information.

The final OGLE-2MASS-WISE AGB sample is produced from the object sample in section 2.2. We apply the point source saturation limits of $[W1/W2/W3/K_s] < [2.0/1.5/-3.0/8.5]$. We also enforce, in order, the 5σ faint limits for $[W1/W2/W3/K_s] < [16.83/15.6/11.32/15.5]$. The WISE

[4] http://irsa.ipac.caltech.edu/cgi-bin/Gator/nph-scan?mission=irsa&submit=Select&projshort=WISE

point source saturation and 5σ faint limits can be found in Cutri et al. (2012). The 2MASS faint and saturation limits are found in Skrutskie et al. (2006). To ensure quality measurements in the desired bands, we also enforce $[W1/W2/W3]$ SNR > 3, and contamination & confusion flags (`cc_flag`) set to 0 in each of those bands. The VAGC, LRG, and YSO samples are filtered through the same criteria. Note that we deliberately neglect $W4$ because, after applying the 5σ faint limits as well as `cc_flag`=0, our sample is too heavily reduced. The resulting populations from each reduction step can be found in Table 1.

Population	OGLE	QSO	AGN	SF	SB	LRGs	YSOs	Locus	RGBs	**Total**
Original	46,467	122,550	19,184	232,845	67,128	105,631	290	25,254	45,528	**664, 877**
WISE match	43,247	6,902	3,098	36,539	10,359	75,543	274	25,254	40,764	**241, 980**
$W1$-3, K_s sat. limit	43,201	6,900	3,098	36,538	10,358	75,527	214	25,156	40,763	**241, 755**
$W1$-2 faint limit	43,200	6,891	3,098	36,537	10,358	75,527	214	24,382	40,760	**240, 967**
$W1$-3 faint limit	19,358	6,728	3,005	35,678	10,105	1,184	214	3,154	5,170	**84, 596**
$W1$-3, K_s faint limit	19,358	5,283	2,878	34,299	9,676	1,167	213	3,070	5,170	**81, 114**
$W1$-3 SNR > 3	18,995	5,279	2,876	34,285	9,673	1,079	213	3,056	4,727	**80, 183**
cc_flag $= 0$	8,454	5,029	2,741	32,805	9,219	1,038	174	3,056	1,599	**64, 125**

Table 1: Sample populations with respect to each reduction step. Please see section 2.6 for the appropriate saturation limits, faint limits, and WISE matching radii.

3. Object Selection Criteria

In producing our candidate sample, we must consider our likely physical sources of contamination, and how removing those sources reduces the completeness of our criteria. Using the sample sets from Section 2.6, we consider sample completeness and contamination in Section 3.1 and devise simple criteria in WISE-2MASS color-color space. YSOs and RGBs present a special case of IR contaminants, as they are fairly well embedded in the same color-color regions as AGB stars. We consider the special case of YSOs in Section 3.2, developing finer criteria to remove these objects while still preserving as much of the AGB sample as possible. We do the same with RGBs in Section 3.3.

3.1. Completeness and Contamination of Initial Samples

Sample completeness η is defined as

$$\eta = \frac{N - n_{\rm missed}}{N}$$

where N is the total number of objects in the sample, and $n_{\rm missed}$ is the number of objects outside of the applied boundaries. Ivezić et al. (2013) defines sample contamination as

$$\epsilon \quad = \quad \frac{n_{\rm spurious}}{n_{\rm selected}}.$$

where $n_{\rm spurious}$ is the number of spurious sources and $n_{\rm selected} = N + n_{\rm spurious}$. Our primary goal is to get an acceptably low contamination of the AGB sample ($\leq$2% contamination) while still retaining a large number of AGB stars.

The difficulty with determining contamination is that none of the contaminant sample, save for the locus stars, falls within the region occupied by our AGB sample: the LMC. However, knowing that there is essentially a uniform distribution of extragalactic sources on the sky [a citation would be great], we solve for the number density of objects in the 10,417 sq. deg. DR7 footprint. We then scale these number densities up by the ~ 76.5 deg^2 area occupied by the LMC. This should provide a reasonable estimate for the number of sources that we would find within the region of the LMC, and by consequence estimate our final levels of extragalactic contamination in WISE-2MASS color-color space.

We employ the following color criteria to isolate AGB stars from their potential contaminants:

$$(J - K_s) \quad > \quad 1.1 \tag{4}$$

$$0.2 \quad < \quad (W2 - W3) \quad < \quad 2.5 \tag{5}$$

Figure 5 shows completeness distributions for the OGLE-2MASS-WISE AGB sample, and corresponding contamination distributions for the contaminant samples. YSOs are omitted as they were not objects that could be projected to the LMC. Table 2 shows the completeness and contamination fractions for each color criterion. We include the lower limit in $(W2 - W3)$ because, although there's a higher penalty on completeness and a slight increase in contamination, we want to exclude the spike of locus stars with $(W2 - W3) < 0.2$.

Critiera	QSO	AGN	LRG	SF	SB	Locus	RGB	**AGB Completeness**
$(J - K_s) > 1.1$	0.25%	0.13 %	0.08%	0.56%	0.33%	4.86%	9.65%	91.29%
$(W2 - W3) < 2.5$	0.03%	< 0.01%	0.04%	0.05%	0.01%	1.73%	7.41%	90.03%
$(W2 - W3) > 0.2$	0.03%	< 0.01%	0.05%	0.06%	0.02%	1.83%	7.94%	83.13%

Table 2: Sample contamination and completeness (*bold*) with respect to each successive cut on WISE-2MASS color.

Figure 6 shows the distribution of recovered AGB stars on the sky as well as in color-color space. We reserve a full accounting of YSOs and RGBs for the next subsections, as there is significant overlap between YSOs, RGBs, and AGBs, and they are not evenly distributed across the sky.

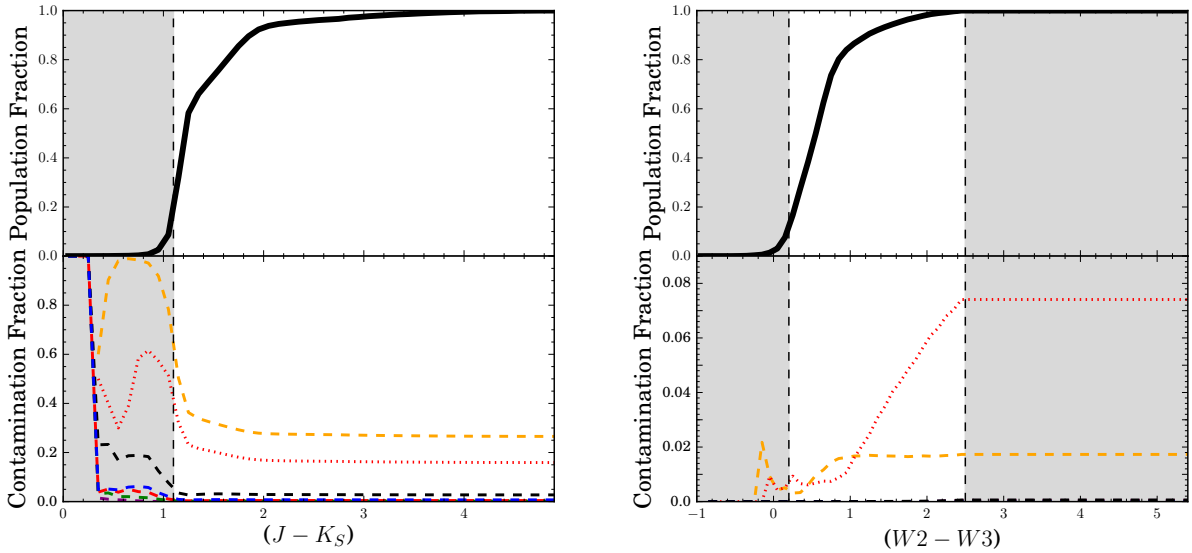

Fig. 5.— *Left:* Cumulative completeness and contamination distributions before $(J - K_s)$ color cut. *Right:* Cumulative completeness and contamination after $(J - K_s)$ and $(W2 - W3)$ cuts. Thick black line in top panels is OGLE-2MASS-WISE AGB completeness as a function of color. The bottom panels show the contamination distributions with respect to color for stellar locus stars (*orange, dashed*), RGB stars (*red, dotted*), LRGs (*purple, dashed*), QSOs (*red, dashed*), AGN (*green, dashed*), starforming galaxies (*black, dashed*), and starburst galaxies (*blue, dashed*). Bin width for both panels is 0.1 dex. Shaded regions represent the color-color space affected by equations 4 & 5.

3.2. Accounting for YSOs

YSOs often directly overlap with AGB stars in WISE color-color space, so we treat these objects separately from our extragalactic contaminants. Rebull et al. (2011) produced a catalog of YSOs in the Taurus Molecular Cloud to bring the total number of YSOs in that region up to 290. We use these and the AGB candidate criteria from Section 3.1 to further refine our criteria and increase the purity of our sample.

Figure 7 shows these 290 YSOs in the field of the Taurus Molecular Cloud, overplotted on WISE objects in that field. As shown in Table 1, after photometric and quality cuts we are left with 174 YSOs, and only 68 after applying equations 4 & 5. In contrast, applying equations 4 & 5 as well as photometric criteria from Section 2.6 to the WISE field in the Taurus Molecular Cloud yields 2,195 AGB candidates in that field. Figure 8 shows the degree of entanglement in color-color space for YSOs and AGB candidates. However, we note that because these are galactic AGB candidates, and the Milky Way is deficient in C-rich AGB stars [XXX CITATION HERE XXX],

Figure 8 misses the degree to which YSOs contaminate the C-rich sequence of AGB stars. To clarify, we compare Taurus YSOs to AGB stars from the LMC (Figure 9). Based on their positions in color-color space, we add three more constraints to remove YSOs from our AGB candidate sample:

$$(W1 - W2) < 0.75(W2 - W3) - 0.33 \quad \text{for } (W2 - W3) > 1.075 \tag{6}$$

$$(W1 - W2) > -(W2 - W3) + 1.5 \quad \text{for } (W2 - W3) > 1.075 \tag{7}$$

$$(W1 - W2) > 0.2 \quad \text{for } (W2 - W3) > 1.3 \tag{8}$$

Collectively, these criteria preserve the C-rich AGB sequence, retain a relatively high completeness fraction for the LMC objects (82.34%), and reduce the sample contamination in the Taurus Molecular Cloud due to YSOs from 1.91% to 0.63%.

3.3. Removing RGBs from WISE Color-Color Space

From [cite that Sosynski paper] we see that in the LMC RGB stars overlap with AGBs in color-color and period-luminosity space, and are very difficult to disentangle from AGB stars. However, they are differentiated by the color-corrected magnitudes of TRGB stars and confidence in a narrow-enough distance distribution that these magnitudes can serve a similar purpose as an absolute magnitude–reference magnitudes where the TRGB can be identified and cut. Since we don't have the luxury of known absolute magnitudes or distances for AGB candidates in the Milky Way, we instead use the OGLE-III RGB sample to estimate where they would be in color-color space.

We begin by convolving the color-color criteria of equations 4 & 5 with the YSO exclusion critieria in 6-8, yielding 603 LMC RGB stars. Even with this grand reduction in the population of RGB stars in our sample, we're still left with 7.97% contamination after excluding YSO stars. This calls for a specific removal of RGB stars from the sample, so we sought to find where they are most concentrated and easiest removed without adversely affecting sample completeness.

Figure 10 shows the distribution of the resulting RGB star sample with respect to the AGB star sample in the LMC in four colors. We find that RGB stars overlap with AGB stars in a narrow sequence with the overwhelming majority falling under $J - K_s < 1.35$. In order to reduce the contamination from these objects in our candidate sample, we impose the following cut:

$$(J - K_s) > 1.35 \text{ for } (W2 - W3) > 0.8. \tag{9}$$

This new criterion results in an LMC AGB star completeness of 71.14%, while reducing the RGB star contamination down to 1.05%. The resulting distribution is seen in Figure 11.

3.4. Post-processing Filter

Using the criteria in equations 4-9, we selected AGB candidates from the ALLWISE-2MASS database. We recovered 1,383,366 candidates, an almost full order of magnitude over the number estimated by [XXX CITE JACKSON, IVEZIC, AND KNAPP 2002XXX] for the entire Milky Way. Suspecting that we hadn't fully accounted for the contribution to the candidate sample from naked stars, we reconcile this discrepancy by adding one final cut motivated by Figure 4 of [XXX CITE NIKUTTA ET AL 2014 XXX]. In that figure, stars from SDSS with $W1 < 15.8$ are plotted in $W1$ vs $(W1 - W2)$, showing a median $(W1 - W2)$ of -0.04 dex. With that in mind, we remove objects with $(W1 - W2) < -0.04$, retaining a final population of 306,793 candidate AGB stars.

4. AGB Candidate Distribution

Having obtained our candidate sample, we validate by observing the spatial distribution of candidate AGB stars throughout the sky. We begin with the distribution of candidates in latitude and longitude, as well as their distributions in notable color-color relationships. Because their NIR brightness is dictated chiefly by the temperatures and compositions of their substantial dusty circumstellar shells, which themselves occupy a narrow range of potential temperatures, we can use their color information and narrow magnitude distribution to produce a color-magnitude relationship for AGB stars and estimate their distances.

We set that stage using known chemically-classified AGB stars from OGLE in the magellanic clouds and find that narrow color-magnitude relationship. We then extend that relationship to our candidate sample, and continue on to produce a three-dimensional map of the galaxy in AGB stars. We discuss the methods involved in that production, the limitations of those methods, and the resulting galactic density distribution of our candidate AGB sample.

4.1. The Full Candidate Distribution

We divide the candidate sample into 6 regions based on galactic position and investigate the resulting galactic and color-color distributions. These distributions can be seen in figures 12 through 17. The positional breakdown of the spatial regions are in Table 3:

What we find is that, regardless of location, Galactic AGB candidates primarily populate the region of W1-W2 vs W2-W3 occupied by O-rich OGLE AGB stars with W1-W2 < 0.4. Additionally the inner 5 kpc contains most of the candidate AGB stars, with 240,881 candidates outside of 20° from the Galactic center.

Region	Description	Count
1	$\|\text{gal } b\| > 5$, $r_{\rm GC} > 20$	22,280
2	$\|\text{gal } b\| < 5$, $r_{\rm GC} > 20$, $\|\text{gal } l\| < 90$	165,886
3	$\|\text{gal } b\| < 5$, $r_{\rm GC} > 20$, $\|\text{gal } l\| > 90$	52,715
4	$r_{\rm GC} < 20$, $r_{\rm GC} > 10$	37,364
5	$r_{\rm GC} < 10$, $r_{\rm GC} > 3$	18,856
6	$r_{\rm GC} < 3$	2,861

Table 3: $r_{\rm GC}$ is the radius from the Galactic center in degrees.

4.2. O-rich and C-rich AGB Candidates

4.3. Galactic Number Density

5. Conclusions

Put words here

REFERENCES

Bahcall, J. N., & Soneira, R. M. 1980, *Ap. J. Suppl.*, 44, 73

Belokurov, V., et al. 2006, *Ap. J. (Letters)*, 642, L137

Benjamin, R. A., et al. 2003, *Pub. A.S.P.*, 115, 953

Berry, M., et al. 2012, *Ap. J.*, 757, 166

Blanton, M. R., et al. 2005, *A. J.*, 129, 2562

Bond, N. A., et al. 2010, *Ap. J.*, 716, 1

Boyer, M. L., et al. 2011, *A. J.*, 142, 103

Churchwell, E., et al. 2009, *Pub. A.S.P.*, 121, 213

Cutri, R. M., et al. 2012, Explanatory Supplement to the WISE All-Sky Data Release Products, Tech. rep.

—. 2013, Explanatory Supplement to the AllWISE Data Release Products, Tech. rep.

Davenport, J. R. A., et al. 2014, *M.N.R.A.S.*, 440, 3430

Eisenstein, D. J., et al. 2001, *A. J.*, 122, 2267

Gilmore, G., Wyse, R. F. G., & Kuijken, K. 1989, *Ann. Rev. Astr. Ap.*, 27, 555

Grillmair, C. J. 2006, *Ap. J. (Letters)*, 651, L29

Habing, H. J., Olnon, F. M., Chester, T., Gillett, F., & Rowan-Robinson, M. 1985, *Astr. Ap.*, 152, L1

Herwig, F. 2005, *Ann. Rev. Astr. Ap.*, 43, 435

Iben, Jr., I., & Renzini, A. 1983, *Ann. Rev. Astr. Ap.*, 21, 271

Ivezić, Ż., Connolly, A., VanderPlas, J., & Gray, A. 2013, Statistics, Data Mining, and Machine Learning in Astronomy

Ivezić, Ž., et al. 2000, *A. J.*, 120, 963

—. 2008, *Ap. J.*, 684, 287

Jackson, T., Ivezić, Ž., & Knapp, G. R. 2002, *M.N.R.A.S.*, 337, 749

Jurić, M., et al. 2008, *Ap. J.*, 673, 864

Kazin, E. A., et al. 2010, *Ap. J.*, 710, 1444

Knauer, T. G., Ivezić, Ž., & Knapp, G. R. 2001, *Ap. J.*, 552, 787

Majewski, S. R. 1993, *Ann. Rev. Astr. Ap.*, 31, 575

Majewski, S. R., Skrutskie, M. F., Weinberg, M. D., & Ostheimer, J. C. 2003, *Ap. J.*, 599, 1082

Matsuura, M., et al. 2005, *Astr. Ap.*, 434, 691

Newberg, H. J., et al. 2002, *Ap. J.*, 569, 245

Nikutta, R., Hunt-Walker, N., Nenkova, M., Ivezić, Ž., & Elitzur, M. 2014, *M.N.R.A.S.*, 442, 3361

Olofsson, H., González Delgado, D., Kerschbaum, F., & Schöier, F. L. 2002, *Astr. Ap.*, 391, 1053

Rebull, L. M., et al. 2011, *Ap. J. Suppl.*, 196, 4

Saito, R. K., et al. 2012, *Astr. Ap.*, 537, A107

Sesar, B., et al. 2010, *Ap. J.*, 708, 717

Skrutskie, M. F., et al. 2006, *A. J.*, 131, 1163

Soszynski, I., et al. 2007, *Acta Astronomica*, 57, 201

Soszynski, I., Udalski, A., Kubiak, M., Szymanski, M., Pietrzynski, G., Zebrun, K., Szewczyk, O., & Wyrzykowski, L. 2004, *Acta Astronomica*, 54, 129

Soszynski, I., et al. 2005, *Acta Astronomica*, 55, 331

Soszyński, I., et al. 2009, *Acta Astronomica*, 59, 239

—. 2011, *Acta Astronomica*, 61, 217

Udalski, A., Szymanski, M. K., Soszynski, I., & Poleski, R. 2008, *Acta Astronomica*, 58, 69

Vivas, A. K., & Zinn, R. 2006, *A. J.*, 132, 714

Vivas, A. K., et al. 2001, *Ap. J. (Letters)*, 554, L33

Wood, P. R., et al. 1999, in IAU Symposium, Vol. 191, Asymptotic Giant Branch Stars, ed. T. Le Bertre, A. Lebre, & C. Waelkens, 151

Wright, E. L., et al. 2010, *A. J.*, 140, 1868

Yanny, B., et al. 2000, *Ap. J.*, 540, 825

York, D. G., et al. 2000, *A. J.*, 120, 1579

Zebrun, K., Soszynski, I., & Wozniak, P. R. 2001, *Acta Astronomica*, 51, 303

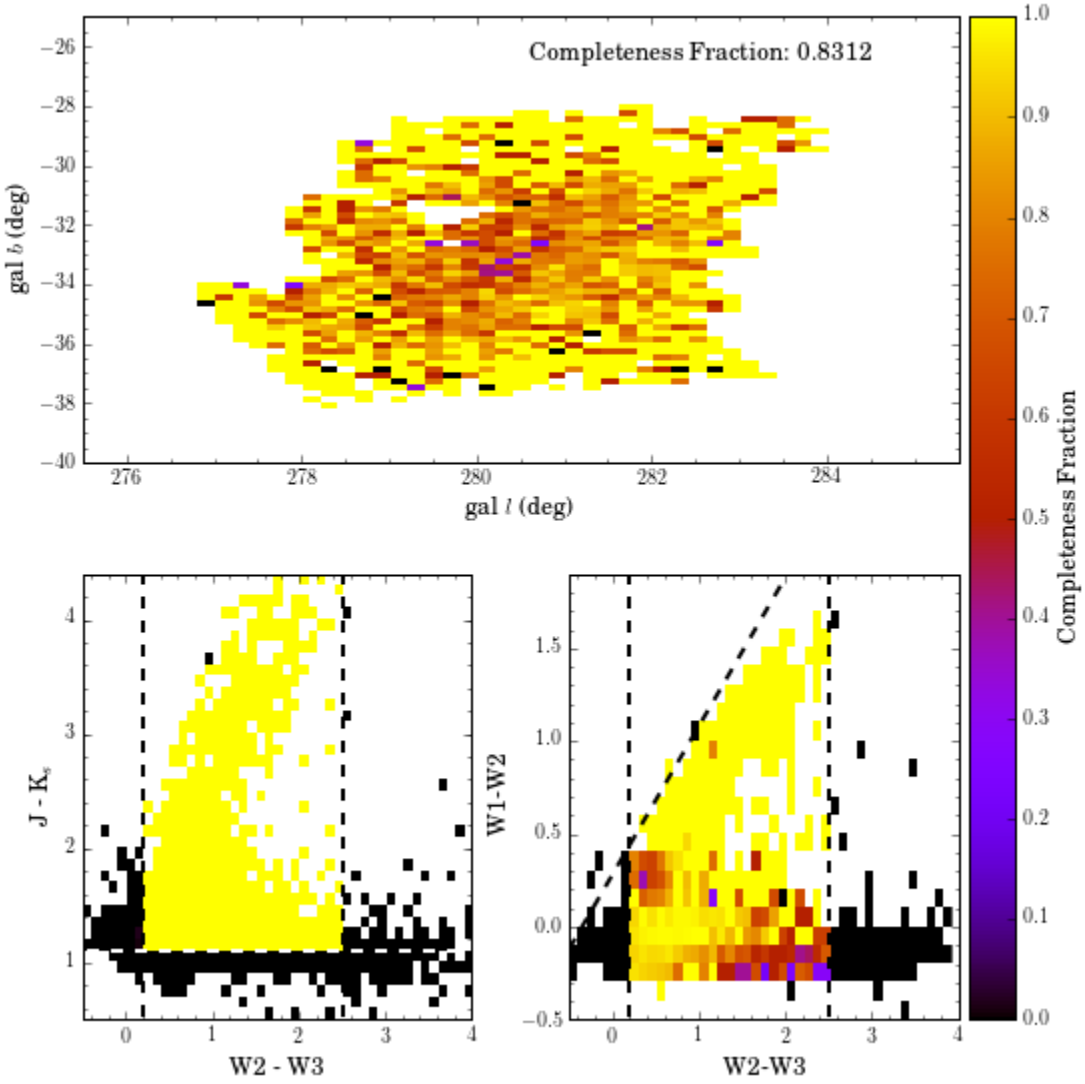

Fig. 6.— Completeness fraction distributions for AGB stars in the LMC. *Top:* OGLE-III AGB completeness fractions with position. Bin size is 0.2 deg on each axis. *Bottom:* completeness fractions in color-color space. Dashed lines represent the primary AGB candidate criteria in equations 4 & 5. Bin size is 0.1 dex on each axis.

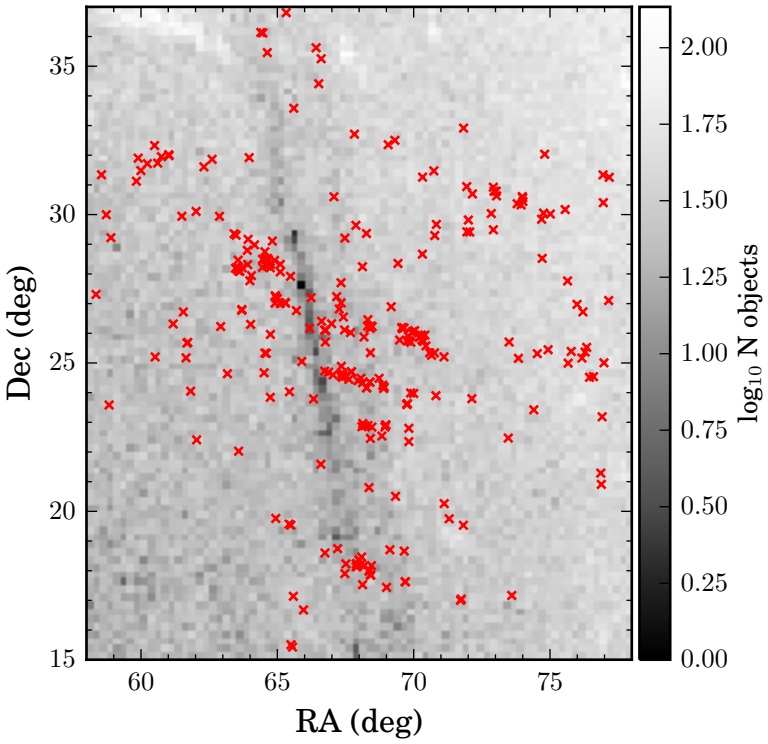

Fig. 7.— YSOs (*red x*) in the Taurus Molecular Cloud (*background*), sampled from (Rebull et al. 2011).

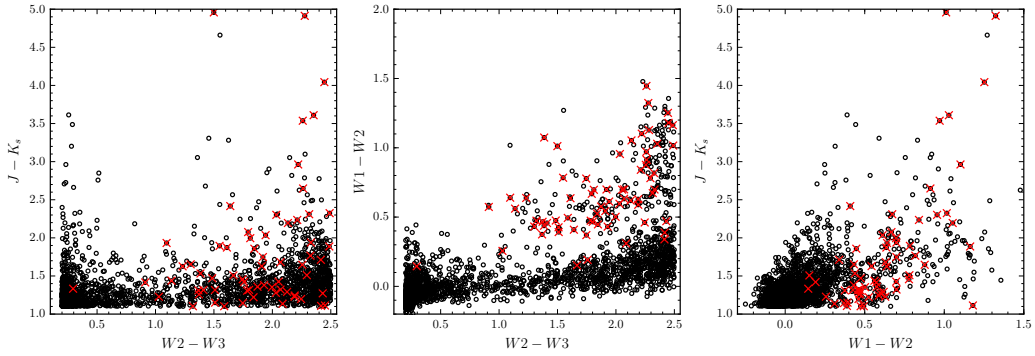

Fig. 8.— YSOs (*red x*) and AGB candidates (*black o*) in the Taurus Molecular Cloud.

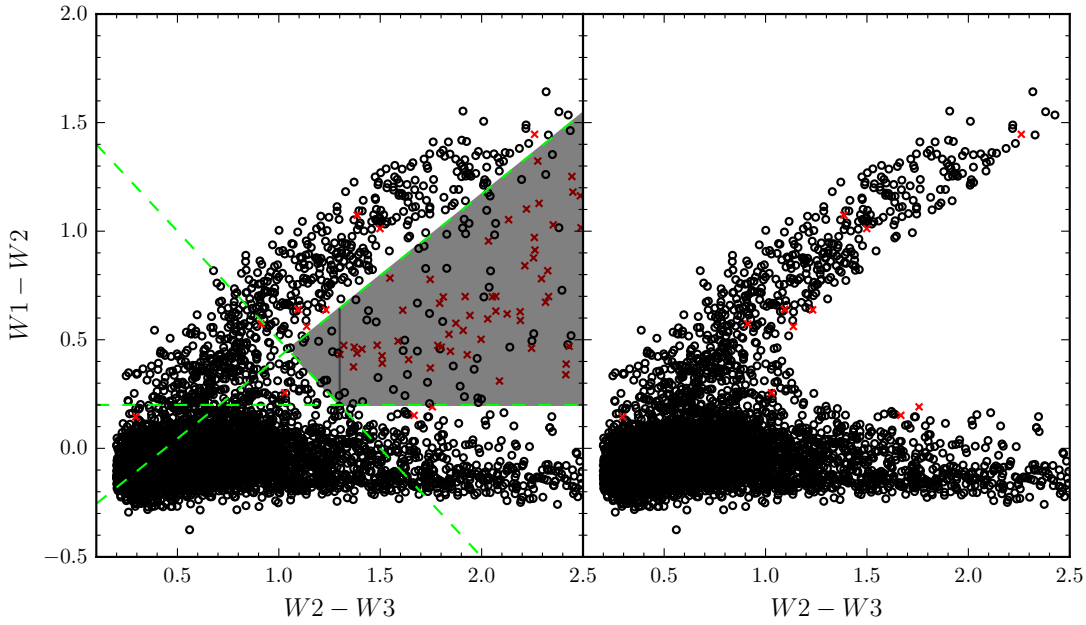

Fig. 9.— YSOs (*red x*) and OGLE-III AGBs (*black o*) in the LMC before (*left*) and after (*right*) the application of YSO exclusion criteria in equations 6-8. Dashed green lines outline the bounds for the YSO exclusion criteria, whose area is shaded in black.

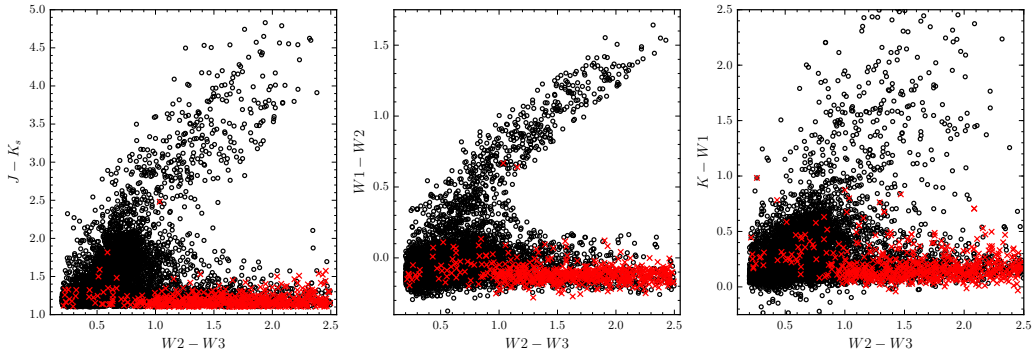

Fig. 10.— OGLE-III RGBs (*red x*) and OGLE-III AGBs (*black dot*) in the LMC.

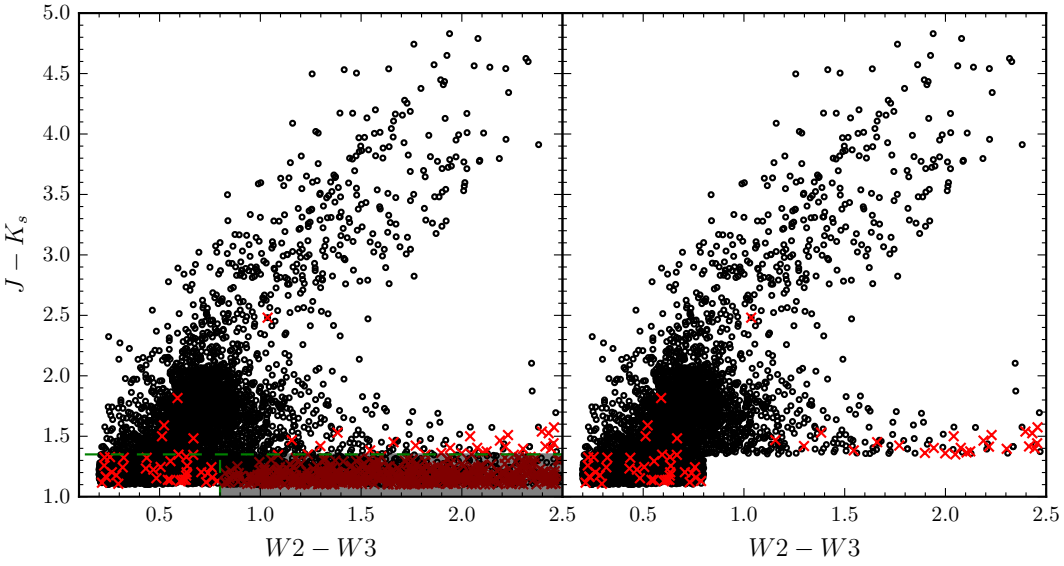

Fig. 11.— OGLE-III RGBs (*red x*) and OGLE-III AGBs (*black dot*) in the LMC before (*left*) and after (*right*) the application of equation 9.

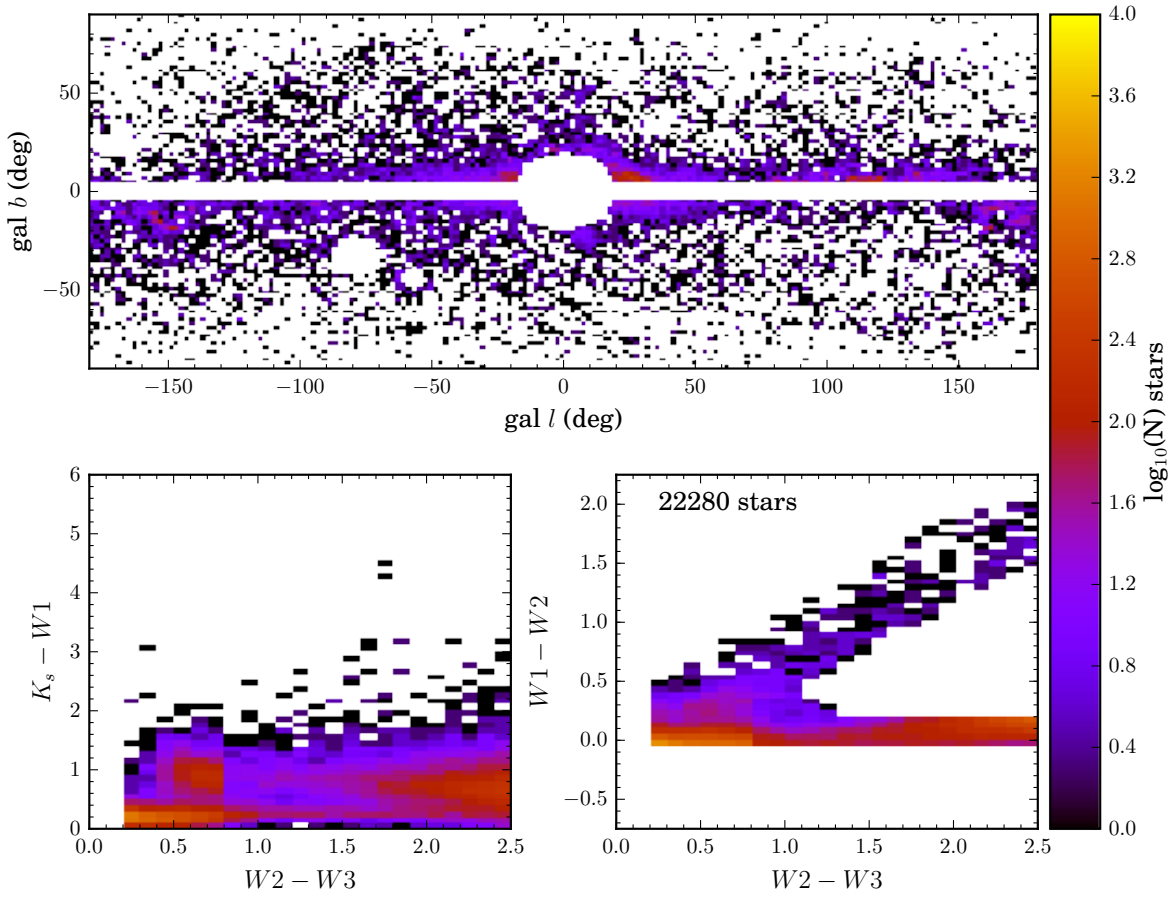
gal b (deg)
gal l (deg)
$\log_{10}$(N) stars
22280 stars
$K_s - W1$
$W2 - W3$
$W1 - W2$
$W2 - W3$

Fig. 12.—

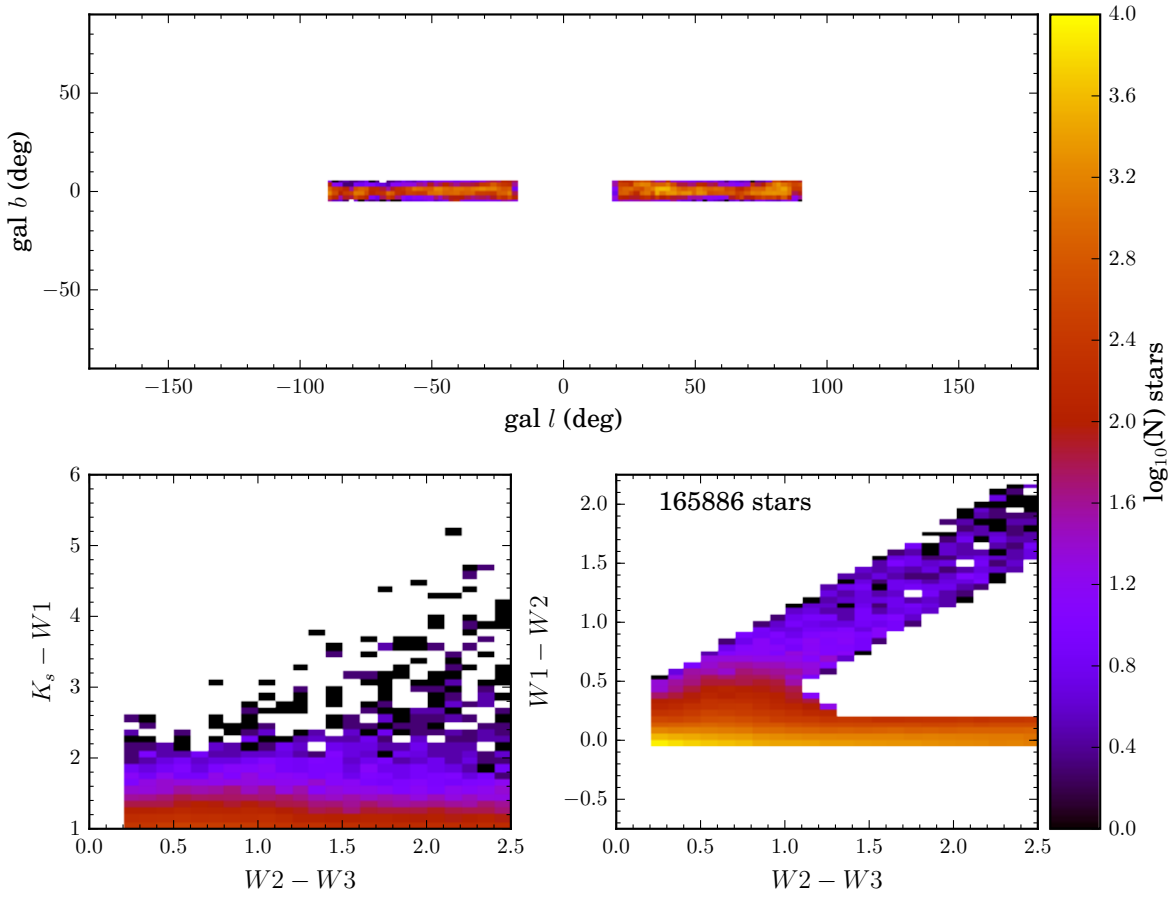
gal b (deg)
gal l (deg)
$\log_{10}$(N) stars
165886 stars
$K_s - W1$
$W2 - W3$
$W1 - W2$
$W2 - W3$

Fig. 13.—

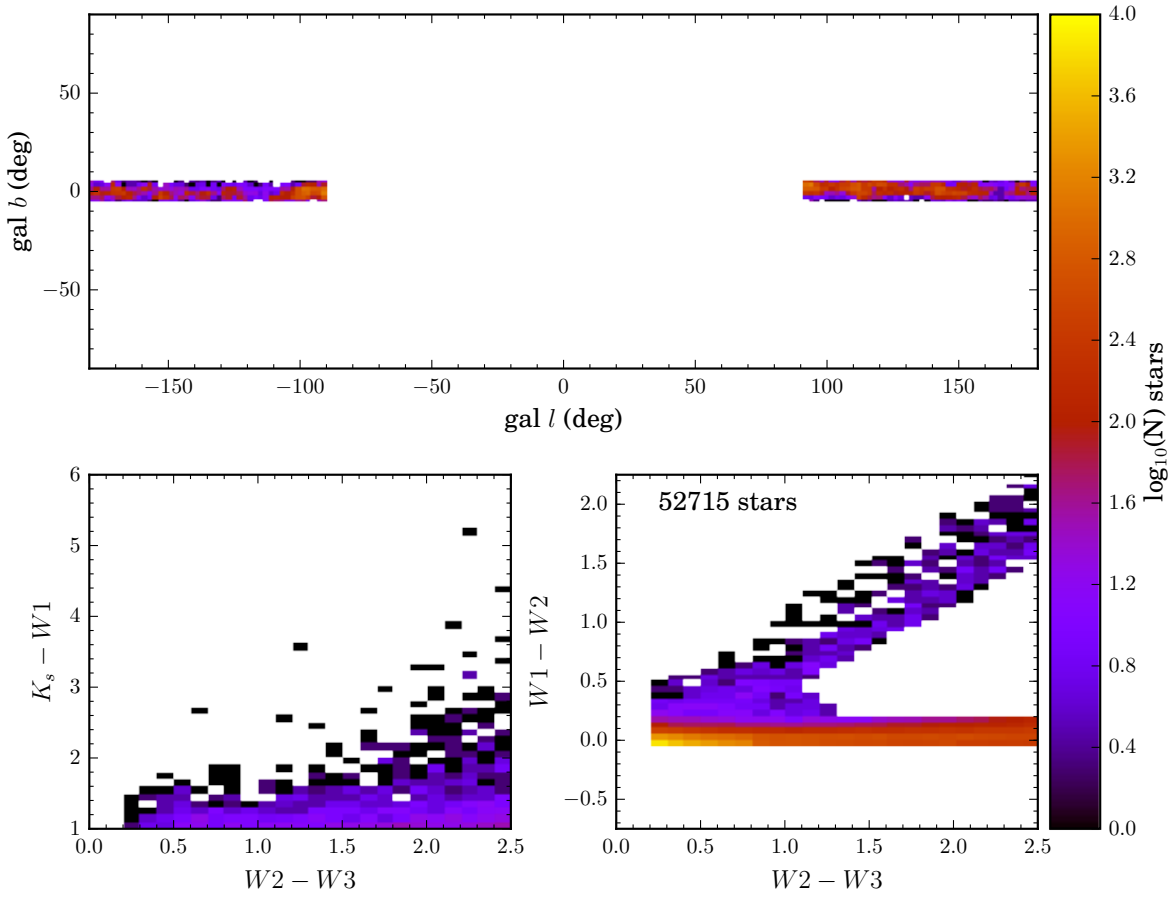
gal b (deg)
gal l (deg)
$K_s - W1$
$W2 - W3$
$W1 - W2$
$W2 - W3$
52715 stars
$\log_{10}$(N) stars

Fig. 14.—

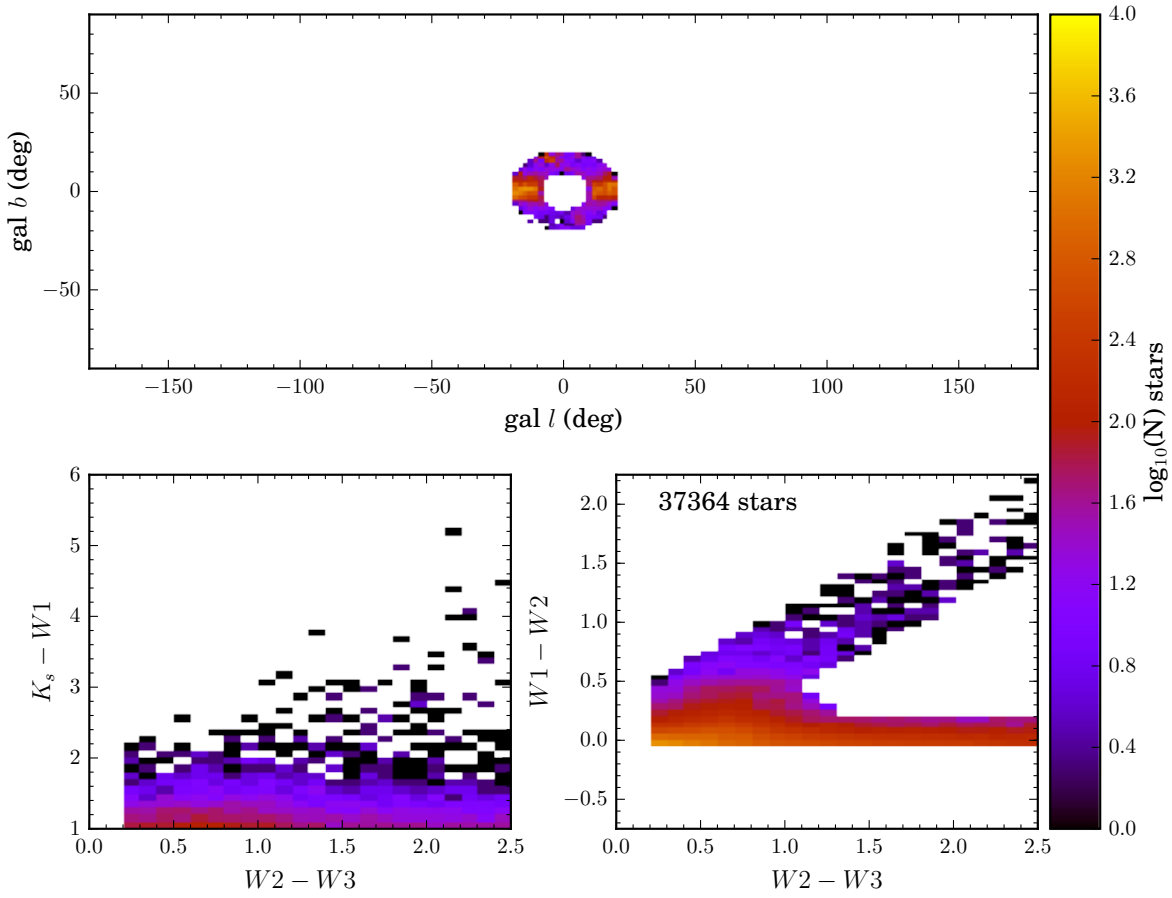
gal b (deg)
gal l (deg)
$K_s - W1$
$W2 - W3$
$W1 - W2$
$W2 - W3$
37364 stars
$\log_{10}$(N) stars

Fig. 15.—

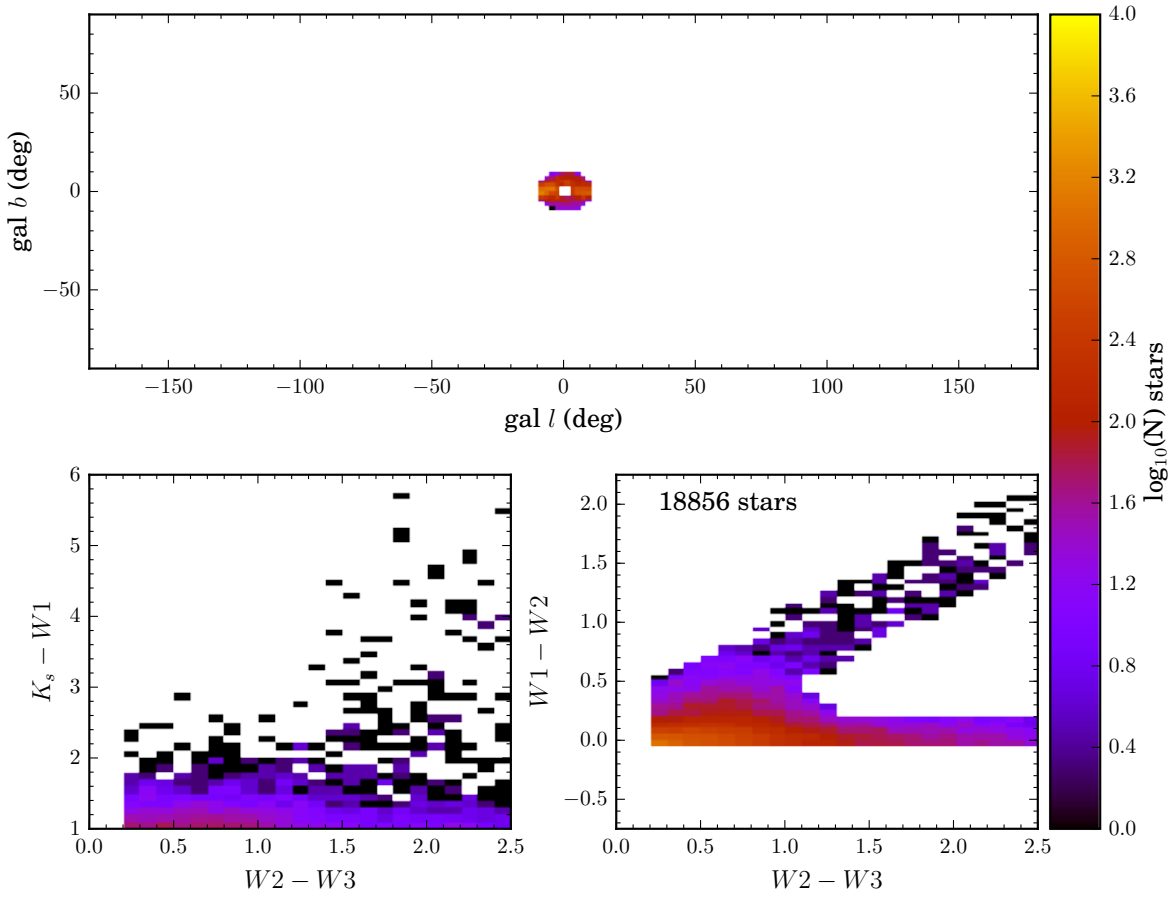
gal b (deg)
gal l (deg)
18856 stars
$K_s - W1$
$W2 - W3$
$W1 - W2$
$W2 - W3$
$\log_{10}$(N) stars

Fig. 16.—

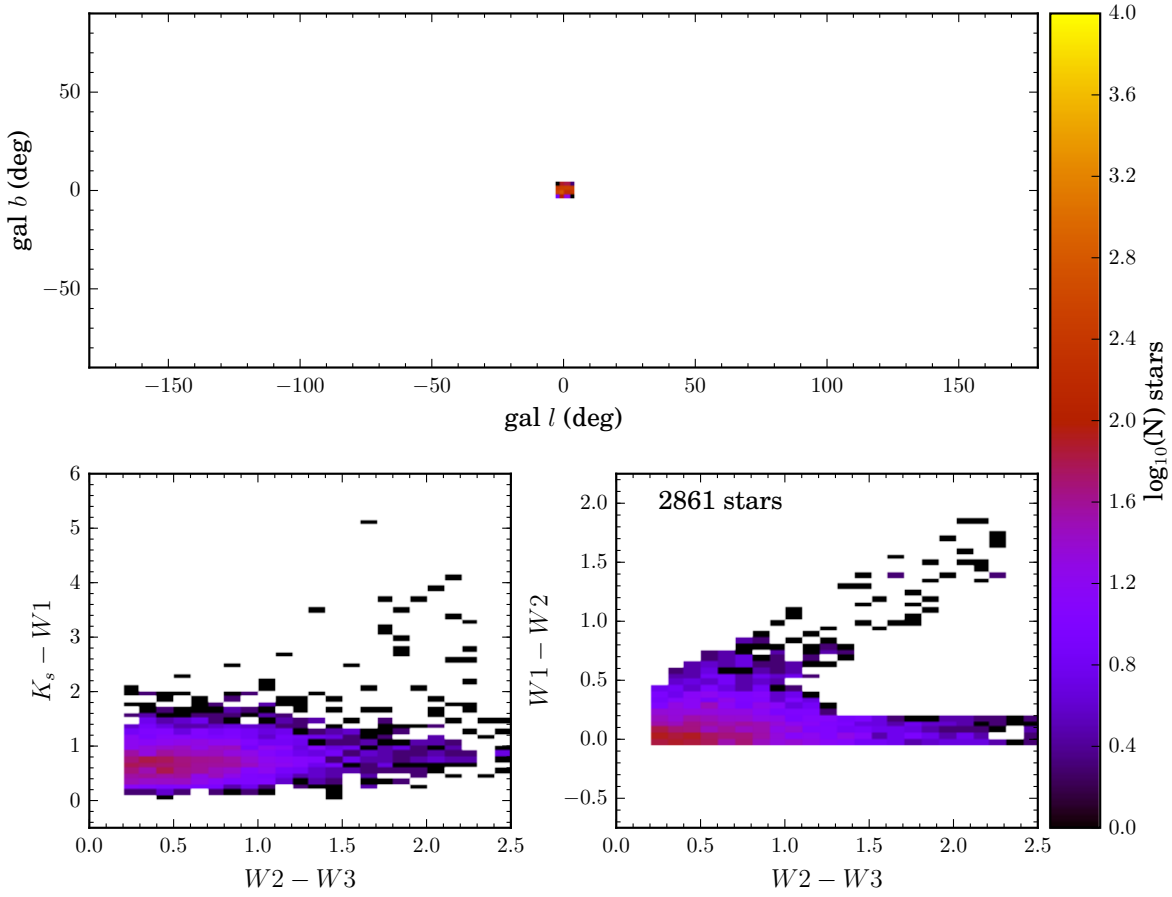
gal b (deg)
gal l (deg)
$K_s - W1$
$W2 - W3$
$W1 - W2$
$W2 - W3$
2861 stars
$\log_{10}$(N) stars

Fig. 17.—